

Variable accretion and emission from the stellar winds in the Galactic centre

Jorge Cuadra^{1,2*}, Sergei Nayakshin³, Fabrice Martins⁴

¹*JILA, University of Colorado and National Institute of Standards and Technology, Boulder, CO 80309-0440, USA*

²*Max-Planck-Institut für Astrophysik, D-85741 Garching, Germany*

³*Department of Physics & Astronomy, University of Leicester, LE1 7RH, UK*

⁴*Max-Planck-Institut für extraterrestrische Physik, D-85741 Garching, Germany*

Accepted XXX. Received XXX; in original form XXX

ABSTRACT

We present numerical simulations of stellar wind dynamics in the central parsec of the Galactic centre, studying in particular the accretion of gas on to Sgr A*, the super-massive black hole. Unlike our previous work, here we use state-of-the-art observational data on orbits and wind properties of individual wind-producing stars. Since wind velocities were revised upwards and non-zero eccentricities were considered, our new simulations show fewer clumps of cold gas and no conspicuous disc-like structure. The accretion rate is dominated by a few close ‘slow wind stars’ ($v_w \leq 750 \text{ km s}^{-1}$), and is consistent with the Bondi estimate, but variable on time-scales of tens to hundreds of years. This variability is due to the stochastic in-fall of cold clumps of gas, as in earlier simulations, and to the eccentric orbits of stars. The present models fail to explain the high luminosity of Sgr A* a few hundred years ago implied by *Integral* observations, but we argue that the accretion of a cold clump with a small impact parameter could have caused it. Finally, we show the possibility of constraining the total mass-loss rate of the ‘slow wind stars’ using near infra-red observations of gas in the central few arcseconds.

Key words: Galaxy: centre – accretion: accretion discs – galaxies: active – stars: winds, outflows

1 INTRODUCTION

Sgr A* is identified with the $M_{\text{BH}} \sim 3.5 \times 10^6 M_\odot$ super-massive black hole (SMBH) at the centre of our Galaxy (e.g., Schödel et al., 2002; Ghez et al., 2005). By virtue of its proximity, Sgr A* may play a key role in the understanding of Active Galactic Nuclei (AGN). Unlike any other SMBH, observations reveal in detail the origin of the gas in the vicinity of Sgr A*. This information is essential for the accretion problem to be modelled self-consistently.

One of Sgr A* puzzles is its very low luminosity with respect to estimates of the accretion rate. Young massive stars in the inner parsec of the Galaxy emit in total $\sim 10^{-3} M_\odot \text{ yr}^{-1}$, filling this region with hot gas. From *Chandra* observations, one can measure the gas density and temperature around the inner arcsecond¹ and then estimate the Bondi accretion rate (Baganoff et al., 2003). The expected

luminosity is orders of magnitude higher than the measured $\sim 10^{36} \text{ erg s}^{-1}$.

The hot gas, however, is continuously created in shocked winds expelled by tens of young massive stars near Sgr A*, and the stars themselves appear to be distributed in two discs (Genzel et al., 2003; Paumard et al., 2006). The situation then is far more complex than in the idealised – spherically symmetric and steady state – Bondi model. An alternative approach is to model the gas dynamics of stellar winds, assuming that the properties of the wind sources are known (Coker & Melia, 1997; Rockefeller et al., 2004; Quataert, 2004; Mościbrodzka et al., 2006). These calculation however did not include the motion of the stars.

Cuadra et al. (2005, 2006) modelled the wind accretion onto Sgr A*, for the first time allowing the wind-producing stars to move, and showed the important influence of the orbits on the accretion. In addition, they found that the winds create a complex two-phase medium and that the accretion rate has a strong variability on time-scales of tens to hundreds of years. The stars, however, were modelled as a group of sources whose features broadly reproduced the observed

* e-mail: jcuadra@jilaui.colorado.edu

¹ One arcsecond ($1''$) corresponds to $\sim 0.04 \text{ pc}$, $\sim 10^{17} \text{ cm}$, or $\sim 10^5 R_S$ for Sgr A*.

distribution of orbits and mass loss properties. In this paper we present our new simulations that treat the stellar population more realistically. We now use the stellar positions and velocities as determined by Paumard et al. (2006), and the wind properties derived by Martins et al. (2007) from the analysis of individual stellar spectra.

This paper starts with a description of our input parameters and a brief account of the simulation method in § 2. In § 3 we characterise the simulated accretion flow in terms of origin, angular momentum, time-variability, and expected X-ray emission. The morphology of the gas on a larger scale and its expected atomic line emission are then explored in §§ 4 and 5. We finally discuss our results in § 6.

2 SIMULATIONS

The simulations were ran using the method described and tested in detail by Cuadra et al. (2006). We use the SPH/*N*-body code GADGET-2 (Springel, 2005) to simulate the dynamics of stars and gas in the gravitational field of the SMBH. To model the stellar orbits more accurately, we also include the gravitational potential of the (old) stellar cusp, as determined by Genzel et al. (2003). The gas hydrodynamics are solved with the SPH (smoothed particle hydrodynamics; e.g., Monaghan, 1992) formulation, in which the gas is represented by a finite number of particles that interact with their neighbours. We include optically thin radiative cooling. The SMBH is modelled as a ‘sink’ particle (Bate et al., 1995; Springel et al., 2005), with all the gas passing within a given distance from it (0.05'' in the present simulations) disappearing from the computational domain. To model the stellar winds, new gas particles are continuously created around the stars.

As wind sources, we include 30 of the stars that Paumard et al. (2006) identify as Wolf-Rayet’s (see Table 1). The remaining two stars, 3E and 7SE2, were not included in the models because of the poor constraints on their orbits. None of these stars is very close to the black hole, nor is there any reason why they should possess larger mass loss rates compared to the other stars². Consequently, we do not expect these two stars to have a strong influence on the accretion rate.

2.1 Stellar wind data

We used the wind properties derived for 18 of the mass-losing stars by Martins et al. (2007). In that study, *H* and *K* band spectra of the Wolf-Rayet stars in the central parsec of the Galaxy were analysed by means of state-of-the-art atmosphere models. Mass loss rates (\dot{M}_w) and terminal wind velocities (v_w) were derived from the strength and width of emission lines. The models assumed inhomogeneous (clumpy) winds, which lead to lower mass loss rates for the 8 stars previously analysed by Najarro et al. (1997) by means of homogeneous models. In addition, wind velocities of stars displaying P-Cygni profiles were found to be larger than in

Table 1. Mass-losing stars and wind properties used in this paper.

ID	Name ‡	v_w km s ⁻¹	\dot{M}_w M _⊙ yr ⁻¹	Note
19	16NW	600	1.12×10^{-5}	1
20	16C	650	2.24×10^{-5}	1
23	16SW	600	1.12×10^{-5}	2
31	29N	1000	1.13×10^{-5}	3
32	16SE1	1000	1.13×10^{-5}	3
35	29NE1	1000	1.13×10^{-5}	3
39	16NE	650	2.24×10^{-5}	4
40	16SE2	2500	7.08×10^{-5}	1
41	33E	450	1.58×10^{-5}	1
48	13E4	2200	5.01×10^{-5}	1
51	13E2	750	4.47×10^{-5}	1
56	34W	650	1.32×10^{-5}	1
59	7SE	1000	1.26×10^{-5}	1
60	–	750	5.01×10^{-6}	5
61	34NW	750	5.01×10^{-6}	1
65	9W	1100	4.47×10^{-5}	1
66	7SW	900	2.00×10^{-5}	1
68	7W	1000	1.00×10^{-5}	1
70	7E2	900	1.58×10^{-5}	1
71	–	1000	1.13×10^{-5}	3
72	–	1000	1.13×10^{-5}	3
74	AFNW	800	3.16×10^{-5}	1
76	9SW	1000	1.13×10^{-5}	3
78	B1	1000	1.13×10^{-5}	3
79	AF	700	1.78×10^{-5}	1
80	9SE	1000	1.13×10^{-5}	3
81	AFNWNW	1800	1.12×10^{-4}	1
82	Blum	1000	1.13×10^{-5}	3
83	15SW	900	1.58×10^{-5}	1
88	15NE	800	2.00×10^{-5}	1

Notes:

- (‡) IDs and names from Paumard et al. (2006).
- (1) From Martins et al. (2007).
- (2) Use 16NW.
- (3) Use the average of 7W and 7SE.
- (4) Use 16C.
- (5) Use 34NW.

Paumard et al. (2001) because the latter authors used only the emission part of the P-Cygni profile to estimate the terminal velocity of the winds.

For the 12 remaining stars, those not analysed in detail by Martins et al. (2007), we set their wind parameters by simply using those of similar stars that were properly studied. Table 1 shows the list of stars we use with their wind properties.

2.2 Orbital data

For each star we take the current 3D velocity and the position in the sky determined by Paumard et al. (2006). The *z*-coordinate, i.e., its distance from Sgr A* projected along the line of sight, can be chosen using different assumptions for the orbital distribution. We tried a range of reasonable assumptions, described in § 2.2.1 below.

² 7SE2 is a WC9 star very similar to 7W which has $\dot{M} = 10^{-5} \text{ M}_{\odot} \text{ yr}^{-1}$. 3E is a WC5/6 star and Hillier & Miller (1999) derived $\dot{M} = 1.5 \times 10^{-5} \text{ M}_{\odot} \text{ yr}^{-1}$ for a WC5 star.

2.2.1 Different orbital configurations

2.2.1.1 Almost circular orbits The simplest assumption one can make for the stellar orbits is to say they are circular. However, for a given set of values $\vec{v}, x, y, M_{\text{BH}}$ (3D velocity, 2D position, and central mass), it is not possible in general to find a solution z that satisfies at the same time the two requirements for a circular Keplerian orbit: $v^2 = GM_{\text{BH}}/r$ and $\vec{v} \cdot \vec{r} = 0$, where $\vec{r} = (x, y, z)$. Instead, we look for the value of z that minimises the eccentricity, $e = \sqrt{1 + (2\ell^2\epsilon)/(G^2M_{\text{BH}}^2)}$, where $\vec{\ell} = \vec{r} \times \vec{v}$ and $\epsilon = v^2/2 - GM_{\text{BH}}/r$ are the angular momentum and energy per unit mass of the orbiting star, respectively. For the first run, MIN-ECC, we set the current z -coordinate to that value.

2.2.1.2 One stellar disc Levin & Beloborodov (2003) found that many of the young stars in the Galactic centre, those rotating clockwise in the sky, have velocity vectors that lie in a common plane. They interpreted this as a signature that these stars are orbiting Sgr A* in a disc. From updated observations, Beloborodov et al. (2006) estimated the thickness of this disc to be only about 10° and then calculated the most likely z -coordinate for its stars. In our second orbital configuration, 1DISC, we used the z -coordinate calculated in this way by Beloborodov et al. (2006) for the stars they identified as disc members, while for the rest of the stars we use our previous assumption of low eccentricity orbits (§ 2.2.1.1).

2.2.1.3 Two stellar discs Genzel et al. (2003) realised that the majority of the young stars in the Galactic centre are actually confined to two almost perpendicular discs. The second disc, with stars rotating counter-clockwise in the sky, however, is not that well defined, being two times thicker than the clockwise system (Paumard et al., 2006, see also Lu et al. 2006). It is not possible to obtain a robust estimate of the z -coordinate in this case. For definitiveness we simply set $z = -(xn_x + yn_y)/n_z$ for this third orbital configuration, 2DISCS, where (n_x, n_y, n_z) is the vector perpendicular to the best fitting counter-clockwise disc³. For the clockwise rotating stars, we used the Beloborodov et al. (2006) z -coordinates, as described in § 2.2.1.2.

2.2.2 The ‘mini star cluster’ IRS 13E

Two of the wind emitting stars belong to IRS 13E, a group of stars located 0.13 pc away from Sgr A* in projection. The velocities of its components are remarkably similar, so the group appears to be gravitationally bound. Since the SMBH tidal force would quickly disrupt such a group, it is believed that it harbours more mass than what is observed as massive stars, perhaps in the form of an intermediate-mass black hole (Maillard et al., 2004; Schödel et al., 2005; Paumard et al., 2006). To take this into account when calculating the z -coordinate of its components, we replaced their individually measured velocities with the average group motion reported

by Paumard et al. (2006). Moreover, we include in the simulations a $350 M_\odot$ ‘dark matter’ particle to keep the group bound.

2.2.3 Setting the initial conditions

Once the z -coordinates are set using any of the assumptions described above (§ 2.2.1), we ran N -body calculations to evolve the orbits back in time for 1100 yr. The final stellar positions and velocities from those runs were used as initial conditions for the winds simulations.⁴

3 ACCRETION ON TO SGR A*

3.1 Variability and origin of the accretion

We define the accretion rate on to Sgr A* as the rate at which mass enters the inner boundary ($0.05''$) of our computational domain. The upper panel of Fig. 1 shows the so-defined accretion rate for run MIN-ECC, where the orbits were made as circular as possible. The lower panel shows the distance from the innermost stars to the black hole as a function of time for the same simulation. In this case most of the accreted material comes from the innermost stars 16SW and 16C, whose orbits oscillate in the range ~ 1.5 – $2''$. These stars have relatively slow wind velocities, $v_w \approx 600 \text{ km s}^{-1}$. Additionally, star 33E, that was further away but has even slower winds with $v_w = 450 \text{ km s}^{-1}$, makes an important contribution to the accretion rate. The slow winds from these three stars are captured by Sgr A* more easily than winds from stars like 29N and 16SE1, which were at comparable distances from the black hole, but have faster winds that were not accreted at all.

Figures 2 and 3 show the accretion rate corresponding to runs 1DISC and 2DISCS, respectively. The accretion is again dominated by stars with wind velocities of at most 750 km s^{-1} . The accretion rate history is however different between the simulations. When the orbits are almost circular (Fig. 1), the accretion rate is more stable, with only a few narrow peaks produced by the dense clumps resulting from the cooling of slow winds (see § 4). When the stars are set in one or two discs, the orbits typically have higher eccentricities (notice the variation in the distance vs. time plots), changing the quantity of gas that can be captured by the black hole as a function of time. This is especially true for run 2DISCS, where the innermost star 16NW has quite an eccentric orbit. As a result, when this star approaches the pericentre of its orbit, a large fraction of its winds is captured directly by Sgr A* within our numerical framework.

Cuadra et al. (2006) used only circular orbits and found that, while the total amount of accretion was dominated by hot gas (temperature $T > 10^7 \text{ K}$), the variable accretion rate was mainly caused by the infall of cold clumps. In these new simulations, the accretion is again dominated by hot gas, but there is almost no accretion of cold gas at all. The reason for this difference is most likely the eccentricity of the orbits – closer to the black hole the stars acquire high orbital

³ With this setting, two of the stars (16NW, 29N) would have acquired orbits with pericentres $< 0.1''$, comparable to the size of our inner boundary. To avoid numerical problems, we changed their velocities within the error bars, putting them in orbits that do not take them so close to the black hole.

⁴ We made an additional run starting 3000 yr ago. No significant differences were found, so we concentrate on simulations starting 1100 yr ago in this paper.

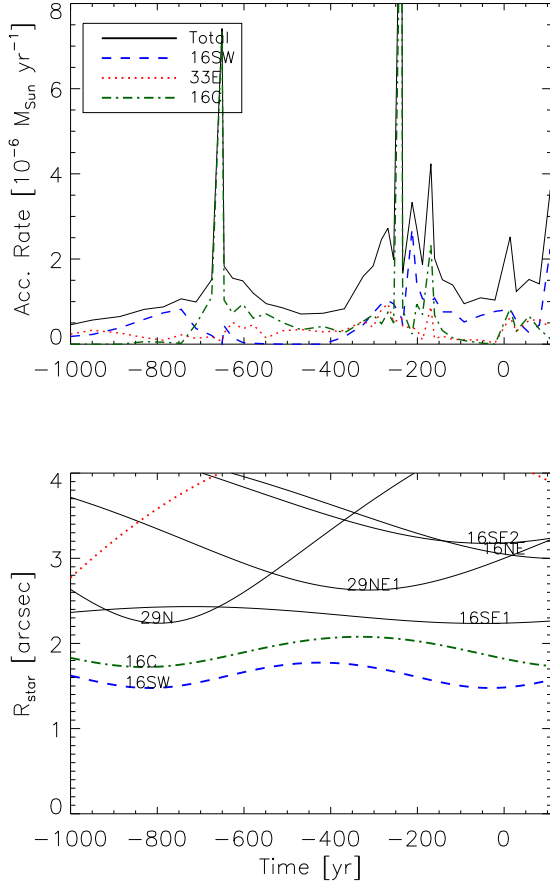


Figure 1. Top panel: Accretion rate as a function of time for run MIN-ECC. The accretion curve is created by sampling the accreted mass every ~ 30 yr and a time value of zero corresponds to the present time. The black solid line shows the total accretion rate while the coloured broken lines show the contribution of the three stars that dominated accretion on to Sgr A* during the simulation. Bottom panel: Distance from the innermost stars to the black hole as a function of time for the same simulation. The curves are labelled with the star names and the three most important stars are shown with the same line properties as in the top panel.

velocities that increase the total velocity of the wind, giving it a large kinetic energy which is then thermalized. Only in the run with orbits closer to circular we see a few sharp peaks in the accretion rate, originated by cold clumps that survived the hot inner region and reached the black hole. On the other hand, the accretion of hot gas shows larger variability than in our previous calculations.

The value of the accretion rate is of the order of a few $\times 10^{-6} M_{\odot} \text{ yr}^{-1}$, consistent with the expectations from the Bondi model (Baganoff et al., 2003). This means that the reason for Sgr A* low luminosity lies in the physics of the inner accretion flow that we cannot resolve with our simulations, and not in how much material is captured by the black hole at distances $\sim 10^4 R_{\text{S}}$.

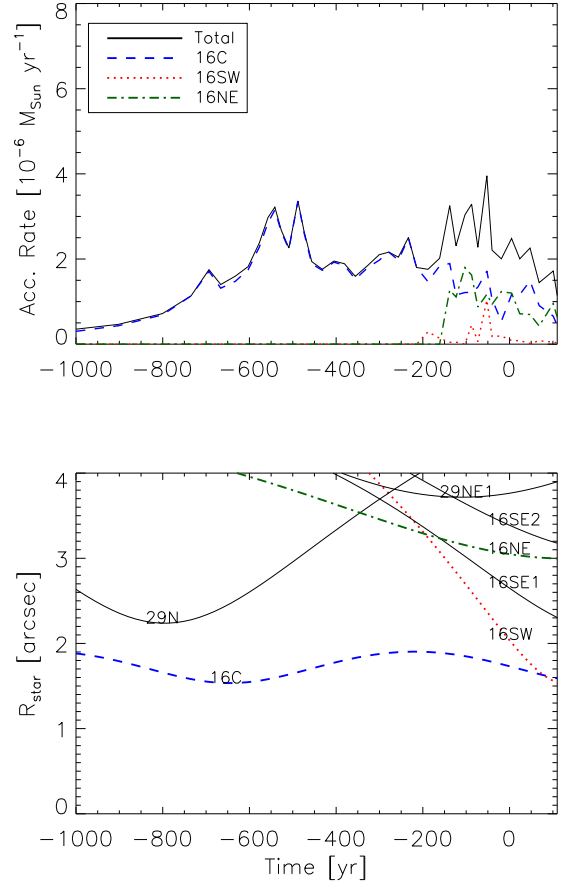


Figure 2. Same as Fig. 1 for run 1DISC.

3.2 Accretion luminosity

We shall try to estimate the X-ray luminosity produced by the accretion flow based on the accretion rate measured at the inner boundary $R = 0.05''$ of the computational domain. Physically, gas that reached this point still needs a time of the order of the flow's viscous time, t_{visc} , to reach Sgr A*. This effect smoothes out any variability in the accretion rate that proceeds on time-scales $\Delta t < t_{\text{visc}}$. Therefore, to calculate the luminosity of the flow we first average the instantaneous accretion rate over time intervals t_{visc} .

From the standard accretion theory (Shakura & Sunyaev, 1973), the viscous time-scale can be estimated as

$$t_{\text{visc}} = \frac{1}{\alpha \Omega_K} \left(\frac{R}{H} \right)^2 = 6.8 \text{ yr } R_{0.05''}^{3/2} \alpha_{0.1}^{-1} \left(\frac{R}{H} \right)^2, \quad (1)$$

where $\alpha = 0.1 \alpha_{0.1}$ is the standard viscosity parameter, Ω_K is the Keplerian orbital frequency, $R = 0.05'' R_{0.05''}$ is the distance from the black hole, and H is the disc thickness. If we take $\alpha = 0.1$, and a geometrically thick disc, $H/R \approx 1$, appropriate for radiatively inefficient accretion, the viscous timescale can be as short as $t_{\text{visc}} \approx 5$ yr. While for a thin disc this timescale can be of course much longer, we concentrate in the $t_{\text{visc}} \sim 5$ yr regime.

The radiative efficiency of the flow is highly uncertain. We therefore use two prescriptions for the X-ray luminosity

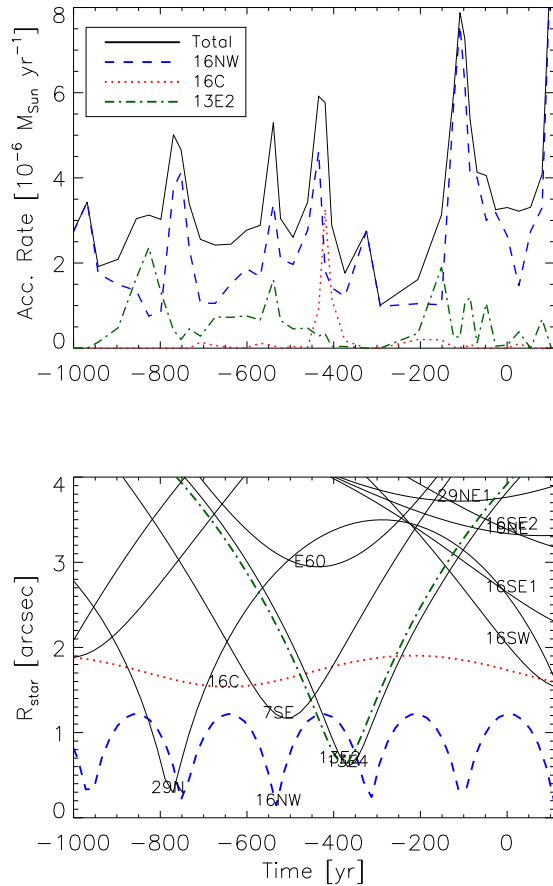


Figure 3. Same as Fig. 1 for run 2DISC.

of the accretion flow L_X as a function of the accretion rate \dot{M} ,

$$L_X = 0.01 \left(\frac{\dot{M}}{\dot{M} + \dot{M}_{\text{crit}}} \right)^\beta \dot{M} c^2, \quad (2)$$

where the parameter β is set to either 1 or 2 and c is the speed of light. This formula provides a smooth transition between the high accretion rate regime, where L_X is expected to be proportional to \dot{M} , and the low accretion rate limit, where the luminosity dependence on \dot{M} is steeper (see, e.g., Merloni et al., 2003, about these two regimes). The critical value of the accretion rate, where it would switch between these regimes, is set at $\dot{M}_{\text{crit}} = 0.01 \dot{M}_{\text{Edd}} \approx 7.7 \times 10^{-2} M_\odot \text{ yr}^{-1}$, as suggested by the study of different modes of accretion in AGNs (e.g., Maccarone et al., 2003).

As an example, we show in Fig. 4 the resulting X-ray luminosity of run 1DISC. As can be seen from the figure, the choice $\beta = 1$ gives a typical luminosity for Sgr A* that is too large compared with the $\sim 2 \times 10^{33} \text{ erg s}^{-1}$ currently observed. The case $\beta = 2$ gives more reasonable results, with typical values $L_X \sim 10^{33} - 10^{34} \text{ erg s}^{-1}$, and is actually closer to the relation ($L_X \propto \dot{m}^{3.4}$) calculated for very inefficient accretion by Merloni et al. (2003).

Interestingly, our simulations show that in the recent past Sgr A* X-ray luminosity could have reached more than $10^{37} \text{ erg s}^{-1}$. On the observational side, Revnivtsev et al.

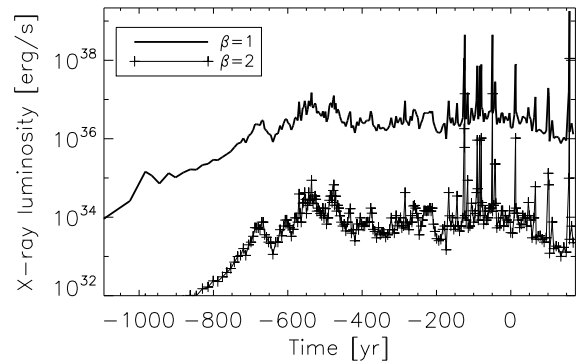


Figure 4. Luminosity from the accretion flow in run 1DISC. The solid and crossed lines correspond to the estimates with $\beta = 1, 2$, respectively.

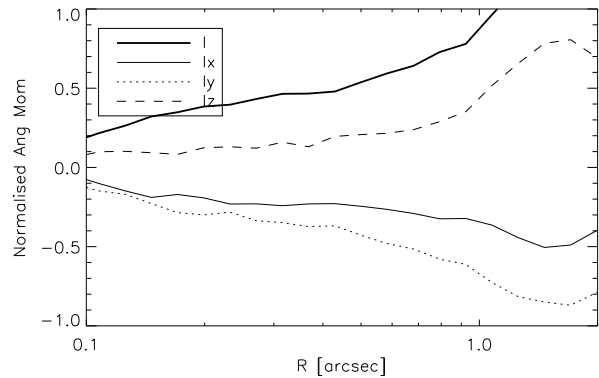


Figure 5. Spherically averaged angular momentum profile of the inner region of the accretion flow of the simulation MIN-ECC. The profile is built using several snapshots in the range $t \approx 0 \pm 37 \text{ yr}$.

(2004) detected hard X-rays from molecular clouds in the vicinity of Sgr A* with *Integral*, and interpreted them as reflection from a bright source, implying a past luminosity of $\sim 10^{39} \text{ erg s}^{-1}$ for Sgr A* that lasted at least a dozen years. It seems difficult to reproduce such high values with our models, especially because tweaking the viscous time-scale to make the peaks higher would at the same time make them narrower than the required duration. However, low mass gas clumps are obviously under-resolved in our simulations at some level. It is possible that the in-fall of a particularly low angular momentum clump much closer in to Sgr A* than our inner boundary radius would result in a flare with the observed characteristics (see § 6).

3.3 Angular momentum and circularisation radius

One important piece of information to characterise the accretion on to Sgr A* is the angular momentum of the gas that it accretes. Figures 5–7 show the angular momentum profile of the three different simulation at $t \approx 0$, corresponding to the present time. The gas close to our inner boundary has an average angular momentum $\ell \approx 0.25$, in units where a circular Keplerian orbit at $R = 1''$ would have $\ell = 1$. We

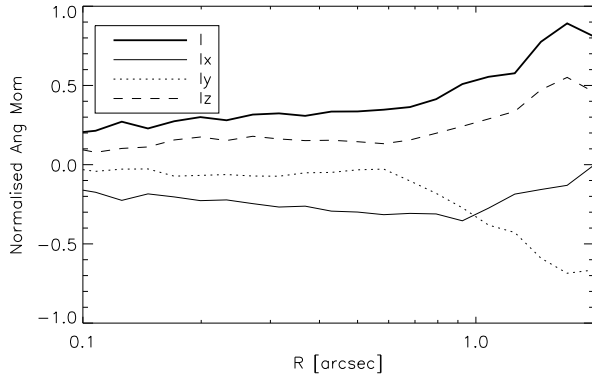


Figure 6. As Fig. 5, but for run 1DISC.

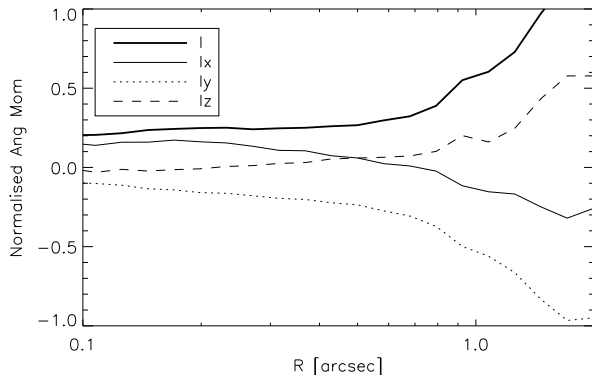


Figure 7. As Fig. 5, but for run 2DISC.

use this value of the angular momentum to roughly estimate at which distance from the black hole the flow will circularise as $R_{\text{circ}} = \ell^2$, which gives $R_{\text{circ}} \sim 0.05'' \sim 5000R_S$ for our simulations. The exact value of circularisation radius is important for modelling the inner accretion flow, and we thus need to examine robustness of our results.

Figure 8 shows the angular momentum values of all SPH particles in the inner $1''$ of the simulation domain. Not surprisingly, at every radius there are very few gas particles that exceed the local Keplerian angular momentum, shown with the solid curve. However, there is significant scatter, i.e., the angular momentum distribution of SPH particles has a significant spread about the mean time-averaged value plotted in Figures 5–7. Without performing a much higher resolution simulation it is difficult to say whether this scatter is real or numerical. In the former case, this would imply that there is a range of angular momentum values for the gas entering the capture radius, and that $\ell \approx 0.25$ is indeed only the average value. We would expect then the gas to circularise over a range of radii, with the circularisation radius $R_{\text{circ}} \sim 0.05''$ representing only a rough geometrical mean value. A further complication is the absence of magnetic fields in our simulations, which could provide means for angular momentum transfer (e.g., Balbus & Hawley, 1998; Proga & Begelman, 2003). Therefore, we conclude that our results on the circularisation radius value are only prelim-

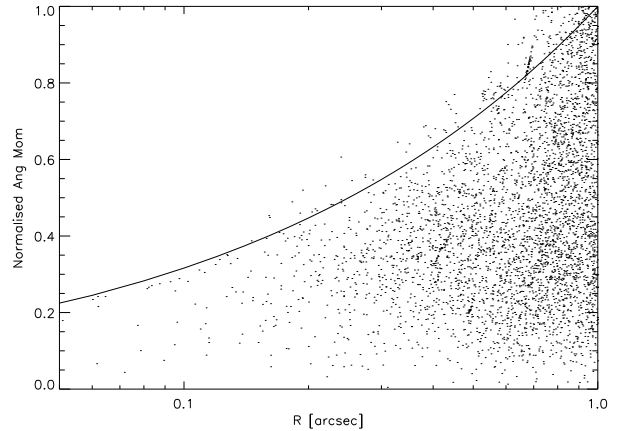


Figure 8. Scatter plot showing the specific angular momentum of every SPH particle in the inner $1''$ for simulation 1DISC at present time ($t = 0$). Very few particles have angular momentum larger than the Keplerian value, shown with the solid line.

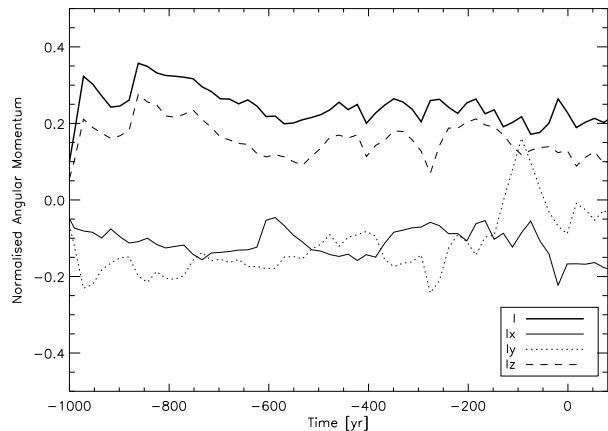


Figure 9. Average angular momentum of the inner $0.3''$ as a function of time from simulation 1DISC.

inary, and more work is needed to pin down its value and dependency on the stellar orbits.

We also plotted the different components of the gas angular momentum (Figs. 5–7). While the magnitude of the specific angular momentum of gas in all the three simulations is similar near the inner boundary, its direction varies significantly. These simulations thus predict different orientations for the midplane of the accretion flow, which is not surprising given a rather significant difference in stellar orbits between the simulations.

The angular momentum also varies as a function of time, as the geometry of the stellar system changes. Fig. 9 shows the average angular momentum of the gas in the inner $0.3''$ as a function of time for the simulation 1DISC. Both the magnitude and the orientation of the angular momentum change by up to a factor 2 on time-scales of tens of years. A sudden change in the angular momentum vector, as that seen in this simulation at $t \approx -100$ yr, can strongly perturb the inner accretion flow and produce an episode of enhanced accretion.

4 GAS MORPHOLOGY

Figure 10 shows the resulting morphology of the gas at present time from run 1DISC. The other two simulations show no important differences, so we concentrate on this intermediate case. The cool and dense clumps originate from the slow winds. When shocked, these slow winds attain a temperature of only around 3×10^6 K, and, given the high pressure environment of the inner parsec of the GC, cool radiatively over a time-scale comparable to the dynamical time (Cuadra et al., 2005). On the other hand, the fast winds do not produce much structure by themselves. This gas reaches temperatures $> 10^7$ K after shocking, and does not cool fast enough to form clumps. This temperature is comparable to that producing X-ray emission detected by *Chandra*. Gas cooler than $\sim 10^7$ K would be invisible in X-rays due to the finite energy window of *Chandra* and the huge obscuration across the Galactic plane.

The new simulations confirm our previous results that the winds create a two-phase medium in the Galactic centre (Cuadra et al., 2006). The quantity of cold gas, however, is very much reduced in the new simulations. We also notice that there is no disc-like structure like the one previously found (Fig. 9 in Cuadra et al., 2006).

There are several reasons for the differences. The wind velocity of the slow wind stars – from whose winds the cold clumps are mostly formed – were revised upward from 300 km s^{-1} to typically 650 km s^{-1} . As the radiative cooling strength for this gas is a strong function of its initial velocity (Cuadra et al., 2005), a much smaller fraction of gas can cool and form clumps. Additionally, the mass loss rates we use for the slow wind stars were revised downward by a factor of a few compared to our previous calculations, so there is even less material that could potentially form clumps.

An et al. (2005) found that Sgr A* flux at $\sim 1 \text{ GHz}$ increased by a factor ~ 2 from 1975 to 2003. These authors attribute the change to a decrease in the free-free opacity produced by a factor 9 change in the column-integrated density squared, $\int n^2 dl$. As it is clear from the density map in Fig. 10, the motion of clumps of gas can easily account for such a change in the obscuration. Further observations should be able to estimate the time-scales on which the change of obscuration happens and therefore confirm the identification of cold clumps with the obscuring material.

5 LINE EMISSION

To compare better the outcome of our simulations with actual observations, we create emission maps of strong near-infrared atomic lines that are expected from gas at $T \sim 10^4$ K. In the simulations the minimum temperature is set to $T = 10^4$ K. This is justified since the powerful UV radiation from the stars in the region ensures that most of the gas remains ionised⁵.

Only a limited comparison with the data is possible at this stage. Our simulations do not include the Mini-spiral, a

rather massive ($\sim 50 M_\odot$) and large scale ionised gas feature composed of several dynamically independent structures (e.g., Paumard et al., 2004). While the origin of the Mini-spiral gas is not quite clear, it seems to follow eccentric orbits originating outside the inner parsec. Fortunately for our study, there does not seem to be much of the Mini-spiral material within few arc-seconds of Sgr A*, so we choose to concentrate on the inner region of the computational domain. Our aim is to find out whether the gas that is produced by the stellar winds would produce a level of emission that is too high compared to the observed value. If that is the case, either the physics of our model is wrong, or the input parameters we are using (stellar properties and orbits) should be revised.

In particular, we create maps of Pa α emission and compare them with the observations of Scoville et al. (2003). We calculate the luminosity per unit volume as

$$4\pi j_{\text{Pa}\alpha} = 6.41 \times 10^{-18} \text{ erg cm}^{-3} \text{ s}^{-1} \left(\frac{T}{6000 \text{ K}} \right)^{-0.87} \left(\frac{n}{10^4 \text{ cm}^{-3}} \right)^2 \quad (3)$$

(Osterbrock, 1989) and then integrate it along the line of sight. An example from simulation 1DISC is shown in Fig. 11. Only a few pixels have a surface brightness comparable to that measured in the Galactic centre inner few arc-seconds (Scoville et al., 2003, their Fig. 7), making the present simulations compatible with the observations. This is in contrast to our earlier simulations (Cuadra & Nayakshin, 2006), the analysis of which shows too much atomic line emission in the near infrared. The difference is not unexpected as the earlier simulations produced much more cold gas in the inner region (see §4).

While a more detailed analysis is left to future work, it is clear that in general the gas luminosity depends on the wind properties. Once more robust orbital data is obtained, it may be possible to constrain the properties of the stellar population, in particular the total mass loss rate from ‘slow wind stars’, using this method that is complementary to the stellar spectra analysis (e.g., Martins et al., 2007).

6 DISCUSSION

We presented our new simulations of stellar wind dynamics in the Galactic centre. We use state-of-the-art data on the stellar orbits (Paumard et al., 2006) and stellar winds properties (Martins et al., 2007). Unfortunately, this does not eliminate the uncertainty in the models completely. The z -coordinate of the stellar wind sources, i.e., the distance along the line of sight to the GC, cannot be obtained observationally. We therefore made several simulations each with a different assumption about the dynamics of these stars, from almost circular orbits to orbits confined in two planes.

The main result of our simulations, compared with results of Cuadra et al. (2005, 2006), is the much smaller quantity of cool gas at $T \lesssim 10^4$ K. We find no cool and geometrically thin disc formed from radiatively cooled stellar winds. This is due to two factors. Firstly, the updated stellar wind velocities are significantly higher, implying that radiative cooling time becomes too long for the shocked winds to form cool clumps. Secondly, the orbits of the important mass losing stars are less disc-like, i.e. circular and coplanar, compared with most of our previous tests.

⁵ For one single star with ionising radiation rate $Q = 10^{48} Q_{48} \text{ s}^{-1}$, the Strömgren radius is $1.38 \text{ pc } Q_{48}^{1/3} n_2^{-2/3}$.

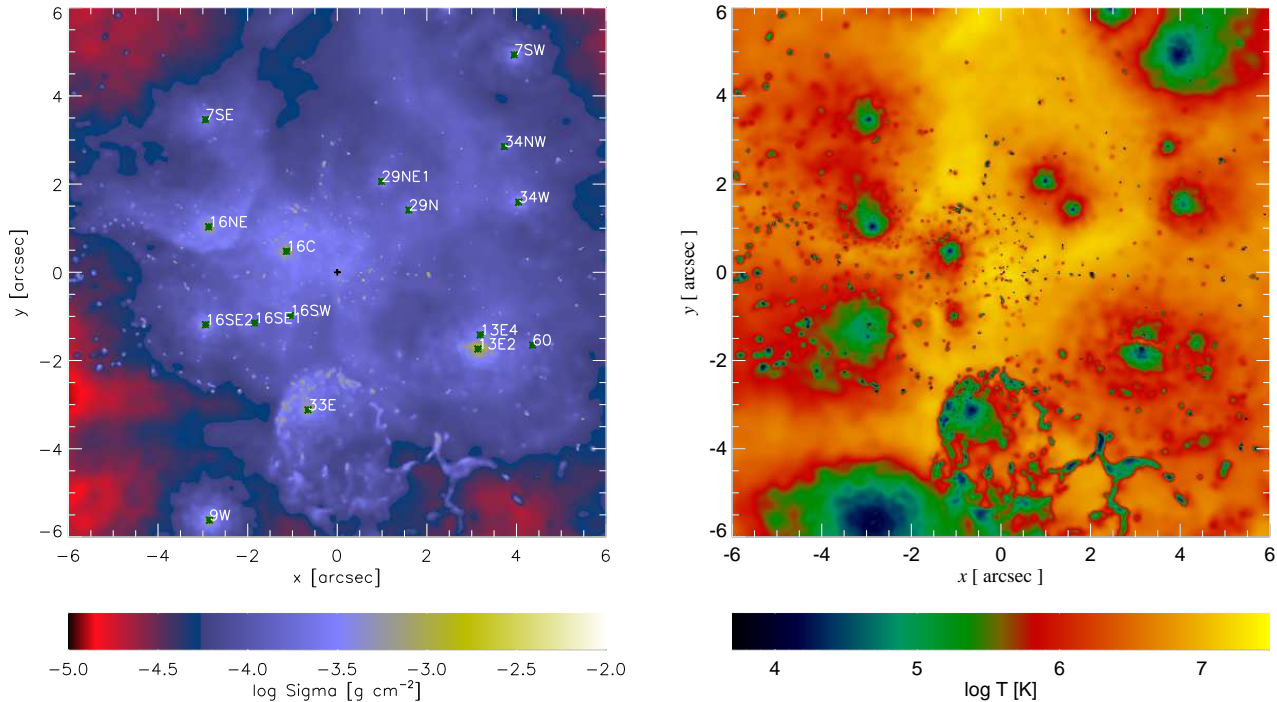


Figure 10. Gas morphology at the present time ($t = 0$) from the simulation 1DISC. Left panel: Column density of gas in the inner $6''$ of the computational domain, as it would be observed from Earth. Stars are shown with green symbols, with labels indicating their names. Right panel: Averaged temperature of the same region. Notice the dense cold clumps forming around the slow-wind-emitting star 33E. Clumps also form in the region around the 13E group, where the slow winds from 13E2 collide with the faster ones coming from its neighbour 13E4. On the other hand, winds from the powerful WR star 9W have not collided yet with any other winds and remain cold but diffuse.

On the other hand, similar to the results of Cuadra et al. (2005, 2006), we find a substantial time variability in the accretion rate histories for Sgr A* in the three different models explored here. In the simulation with small eccentricities (MIN-ECC) the accretion is relatively constant, except for the episodic in-fall of cold clumps that produce sharp peaks in the accretion rate. When the orbits are preferentially in one or two planes (simulations 1DISC and 2DISCS), stars acquire higher eccentricities. The accretion rate history is then strongly variable on a time-scale of tens to hundreds of years mainly due to stars on eccentric orbits. The accretion rate peaks are nearly coincident with times when these stars are at pericentres of their orbits. One should notice however that in the simulation 2DISCS the star 16NW gets uncomfortably close to the inner boundary of the computational domain (Fig. 3), so higher resolution studies are needed to quantitatively confirm the obtained accretion rate. Previous studies have also found substantial variability of the accretion flow, e.g., Proga & Begelman (2003), using MHD models for the region closer to the central black hole (see also Moscibrodzka et al., 2007).

Even though the accretion history looks quite different between the simulations, the average accretion rates are the same within a factor of 2–3. In particular, time-averaged accretion rates of all of the simulations are consistent with the Bondi estimate. This is not unexpected. The capture radius of the wind is around $0.5''$ to $1''$. At these radii, the angular momentum of the gas is well below its Keplerian circular

value. Therefore, rotational support of the flow is unimportant, and the Bondi approximation is valid at these radii. On the other hand, had we been able to resolve and properly model much smaller scales, the angular momentum effects would be considerably more important. This is exactly the direction in which this work needs to be extended to connect it with the radiatively-inefficient accretion flow (RIAF) models that have been developed for Sgr A*. In these models only a small fraction of the energy of the accretion flow is radiated away, allowing them to successfully account for Sgr A* dimness (e.g., Narayan, 2002; Yuan et al., 2003). Also, most of the gas captured by Sgr A* on arc-second scales does not get accreted but rather outflows. In addition to improved numerical resolution, magnetic fields need to be included to account for angular momentum transfer in the flow.

The angular momentum of the accretion flow in the sub arc-second region appears to be similar for the different orbital configurations we tried, with the average circularisation radius being of the order of $\sim 5 \times 10^3$ Schwarzschild radii. This radius is similar to the size of the inner boundary of our simulations. Moreover, its value is calculated from the angular momentum of the gas in the inner region of the computational domain, where the quantity of SPH particles may not be enough to yield robust results. More work is then needed to pin down the exact value of the circularisation radius. Higher numerical resolution – lower SPH particle mass and a smaller value for the inner boundary

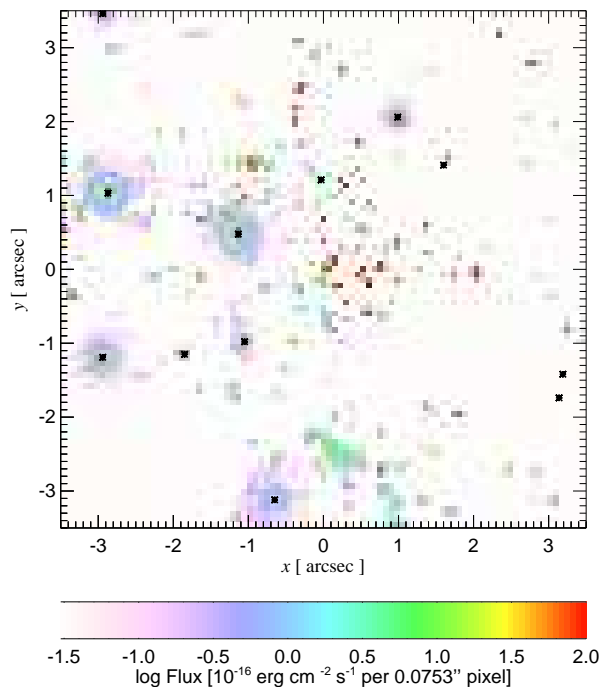


Figure 11. Pa α surface brightness from the stellar winds in run 1DISC, as it would be observed in the sky at present time. The units are those used by Scoville et al. (2003). Stars are shown as black asterisks. The level of emission is too low to be detected on top of the other gas complexes in the GC region.

radius – may result in a smaller value for the circularisation radius. On the other hand, inclusion of magnetic fields, absent in our present simulations, will allow angular momentum to be transferred in the flow via the magnetorotational instability (e.g., Balbus & Hawley, 1991, 1998), perhaps allowing material with a higher value of angular momentum to be ‘accreted’ within the inner boundary. Hence the estimate for the circularisation radius can in principle shift somewhat in either direction.

Although the angular momentum magnitude is roughly the same, the orientation of the accretion flow mid-plane is different in the three simulations, since it is mostly determined by the orbits of a few of the innermost stars. Better measured velocities and constraints on the accelerations (e.g., Lu et al., 2006) should be obtained during the next years of observations, allowing us to improve the determination of the 3-dimensional orbits and get more definitive answers. Once the orbits are better constrained, one could embark on a more ambitious higher resolution study of the inner accretion flow in an attempt to connect it with the non-radiative models mentioned above, and the observational constraints on the inner accretion flow orientation (e.g., Meyer et al., 2006; Trippe et al., 2007).

In this paper we already attempted some modelling of the inner flow in terms of a very simplified approach in which we estimated the X-ray luminosity *within* our inner boundary (§3.2). We found that in the past Sgr A*’s X-ray luminosity could have been much higher than its present value, and could have varied by several orders of magnitude. Nevertheless, none of the peaks reached the $\sim 10^{39}$

erg s $^{-1}$ needed to explain the putative flare in Sgr A* X-ray luminosity a few hundred years ago (Revnivtsev et al., 2004, see also Munro et al. (2007)). However, it is possible that a cold clump falling into the inner region, such as those seen as peaks in Fig. 1, had a low enough angular momentum to circularise at a very small radius, $\sim 0.001''$. At that location, the clump mass would be higher than the mass of the non-radiative flow by a few orders of magnitude. Regardless of whether the cold clump is evaporated by the hot flow, or sheared away and mixed with it, in the end there would be much more mass in this region. The accretion flow would then cool quickly, approaching a standard accretion disc configuration. The viscous time of this flow can be quite long, of the order of 100 yr for a disc thickness $H/R \sim 0.01$, making Sgr A* stay in this state until the excess mass is accreted. Assuming a maximum radiative efficiency for this kind of flow, the bolometric luminosity would be $\sim 10^{40}$ erg s $^{-1}$, enough to give the observed luminosity in the X-rays for the required period of time. We note that there were no such low angular momentum cold clumps in the present simulations, but it is not clear how robust this conclusion is with respect to changes in the model parameters and resolution.

The wind properties we used are based on the spectroscopic study by Martins et al. (2007). The uncertainty of their results is typically only of the order of a few $\times 10\%$, so we did not explore different realisations of the wind data. There is more uncertainty in the wind properties from the 13E group, whose nature is not clearly established yet, and 16SW, which is part of a binary (Martins et al., 2006; Peeples et al., 2007). The analysis of these sources is not yet robust enough and they are important contributors to the accretion. However, we do not expect changes in the results to be larger than those resulting from the different orbital configurations. We can still use our previous work (Cuadra et al., 2005, 2006; Cuadra & Nayakshin, 2006) to understand the effect of changing the wind properties. Clearly, larger mass-loss rates and slower wind velocities produce more gas that is able to cool and form clumps. Too much of that gas can be problematic in the sense that it would overproduce the atomic line emission expected from gas at $T \sim 10^4$ K. The same clumps increase the variability of the accretion rate on time-scales of 10–100 yr.

Our results on the origin of the accreted material differ from those obtained by Mościbrodzka et al. (2006). These authors argued that the accretion on to Sgr A* is dominated by the material expelled by 13E. One reason for the discrepancy is that they used the older values for mass loss rates compiled by Rockefeller et al. (2004), that give a rather extreme value for \dot{M}_{13E} . Mościbrodzka et al. (2006) also neglected the orbital velocity of the innermost stars, that are usually comparable to their wind velocity.

Other models in the literature have focused on the accretion of winds from the OB main sequence stars in the inner arc-second – the ‘S-stars’ (Loeb, 2004; Coker & Pittard, 2005). While the inclusion of these stars would certainly make the models more realistic, their mass loss rates are probably at most $\sim 10^{-7} M_{\odot} \text{ yr}^{-1}$. The star τ Sco has a spectral type (B0.2V) similar to S2 and the estimates of its mass loss rate range from $6 \times 10^{-8} M_{\odot} \text{ yr}^{-1}$ (Mokiem et al., 2005) down to $< 6 \times 10^{-9} M_{\odot} \text{ yr}^{-1}$ (Zaal et al., 1999). Since mass loss rates are known to scale with luminosity (Kudritzki & Puls, 2000) and S2 is the brightest of

the S stars, all of them should have very low \dot{M}_w . Hence, we believe that the effect of the S stars would not affect our conclusions.

ACKNOWLEDGMENTS

We acknowledge useful discussions with T. Paumard on the stellar orbits and the observability of the gas emission, and with F. Yuan on RIAF models. We thank P. Arévalo for proof-reading the draft and the referee for suggestions that significantly improved the paper. JC acknowledges support from NASA Beyond Einstein Foundation Science grant NNG05GI92G. FM acknowledges support from the Alexander von Humboldt foundation. The simulations were performed on the JILA Keck-cluster, sponsored by the W. M. Keck Foundation. Earlier calculations were ran at the Rechenzentrum Garching and at the University of Leicester. JC acknowledges the hospitality of the Theoretical Astrophysics group in Leicester, where part of this work was done.

REFERENCES

- An T., Goss W. M., Zhao J.-H., et al., 2005, *ApJL*, 634, L49
 Baganoff F. K., Maeda Y., Morris M., et al., 2003, *ApJ*, 591, 891
 Balbus S. A., Hawley J. F., 1991, *ApJ*, 376, 214
 Balbus S. A., Hawley J. F., 1998, *Reviews of Modern Physics*, 70, 1
 Bate M. R., Bonnell I. A., Price N. M., 1995, *MNRAS*, 277, 362
 Beloborodov A. M., Levin Y., Eisenhauer F., et al., 2006, *ApJ*, 648, 405
 Coker R. F., Melia F., 1997, *ApJL*, 488, L149
 Coker R. F., Pittard J. M., 2005, in *X-Ray and Radio Connections* (eds. L.O. Sjouwerman and K.K Dyer) Published electronically by NRAO, <http://www.aoc.nrao.edu/events/xraydio> Held 3-6 February 2004 in Santa Fe, New Mexico, USA, (E2.04) 5 pages
 Cuadra J., Nayakshin S., 2006, *Journal of Physics Conference Series*, 54, 436
 Cuadra J., Nayakshin S., Springel V., Di Matteo T., 2005, *MNRAS*, 360, L55
 Cuadra J., Nayakshin S., Springel V., Di Matteo T., 2006, *MNRAS*, 366, 358
 Genzel R., Schödel R., Ott T., et al., 2003, *ApJ*, 594, 812
 Ghez A. M., Salim S., Hornstein S. D., et al., 2005, *ApJ*, 620, 744
 Hillier D. J., Miller D. L., 1999, *ApJ*, 519, 354
 Kudritzki R.-P., Puls J., 2000, *ARA&A*, 38, 613
 Levin Y., Beloborodov A. M., 2003, *ApJ*, 590, L33
 Loeb A., 2004, *MNRAS*, 350, 725
 Lu J. R., Ghez A. M., Hornstein S. D., et al., 2006, *Journal of Physics Conference Series*, 54, 279
 Maccarone T. J., Gallo E., Fender R., 2003, *MNRAS*, 345, L19
 Maillard J. P., Paumard T., Stolovy S. R., Rigaut F., 2004, *A&A*, 423, 155
 Martins F., Genzel R., Hillier D. J., et al., 2007, *A&A*, 468, 233
 Martins F., Tripp S., Paumard T., et al., 2006, *ApJL*, 649, L103
 Merloni A., Heinz S., di Matteo T., 2003, *MNRAS*, 345, 1057
 Meyer L., Schödel R., Eckart A., Karas V., Dovčiak M., Duschl W. J., 2006, *A&A*, 458, L25
 Mokiem M. R., de Koter A., Puls J., Herrero A., Najarro F., Villamariz M. R., 2005, *A&A*, 441, 711
 Monaghan J. J., 1992, *ARA&A*, 30, 543
 Mościbrodzka M., Das T. K., Czerny B., 2006, *MNRAS*, 370, 219
 Moscibrodzka M., Proga D., Czerny B., Siemiginowska A., 2007, *A&A*, 474, 1
 Muno M. P., Baganoff F. K., Brandt W. N., Park S., Morris M. R., 2007, *ApJL*, 656, L69
 Najarro F., Krabbe A., Genzel R., Lutz D., Kudritzki R. P., Hillier D. J., 1997, *A&A*, 325, 700
 Narayan R., 2002, in *Lighthouses of the Universe: The Most Luminous Celestial Objects and Their Use for Cosmology*, edited by M. Gilfanov, R. Sunyaev, E. Churazov, 405
 Osterbrock D. E., 1989, *Astrophysics of gaseous nebulae and active galactic nuclei*, University Science Books
 Paumard T., Genzel R., Martins F., et al., 2006, *ApJ*, 643, 1011
 Paumard T., Maillard J.-P., Morris M., 2004, *A&A*, 426, 81
 Paumard T., Maillard J. P., Morris M., Rigaut F., 2001, *A&A*, 366, 466
 Peebles M. S., Bonanos A. Z., DePoy D. L., et al., 2007, *ApJL*, 654, L61
 Proga D., Begelman M. C., 2003, *ApJ*, 592, 767
 Quataert E., 2004, *ApJ*, 613, 322
 Revnivtsev M. G., Churazov E. M., Sazonov S. Y., et al., 2004, *A&A*, 425, L49
 Rockefeller G., Fryer C. L., Melia F., Warren M. S., 2004, *ApJ*, 604, 662
 Schödel R., Eckart A., Iserlohe C., Genzel R., Ott T., 2005, *ApJL*, 625, L111
 Schödel R., Ott T., Genzel R., et al., 2002, *Nature*, 419, 694
 Scoville N. Z., Stolovy S. R., Rieke M., Christopher M., Yusef-Zadeh F., 2003, *ApJ*, 594, 294
 Shakura N. I., Sunyaev R. A., 1973, *A&A*, 24, 337
 Springel V., 2005, *MNRAS*, 364, 1105
 Springel V., Di Matteo T., Hernquist L., 2005, *MNRAS*, 361, 776
 Tripp S., Paumard T., Ott T., et al., 2007, *MNRAS*, 375, 764
 Yuan F., Quataert E., Narayan R., 2003, *ApJ*, 598, 301
 Zaal P. A., de Koter A., Waters L. B. F. M., et al., 1999, *A&A*, 349, 573